Energy Consumption in Wireless Systems Equipped with RES, UAVs, and IRSs

Adam Samorzewski

Institute of Radiocommunications, Poznań University of Technology, Poznań, Poland

https://doi.org/10.26636/jtit.2023.170923

Abstract — This paper investigates energy budget characteristics of mobile base stations (BSs) having the form of unmanned aerial vehicles (UAVs) equipped with radio frequency (RF) transceivers, intelligent reconfigurable surfaces (IRSs), and renewable energy sources (RES). The results obtained highlight the benefits and challenges related to using the aforementioned mobile BS, from the energy-related point of view. The specific cases researched involved two types of UAV devices, i.e. multirotor and fixed-wing (airplane-like) aircraft.

Keywords — 6G, intelligent reconfigurable surfaces, power consumption, renewable energy sources, unmanned aerial vehicles, wireless systems.

1. Introduction

In recent years, harvesting energy from the sun has become a very common solution used not only in the industrial sector but also in many different areas of our everyday lives. Solar energy is generated by the so-called photovoltaic (PV) panels. The current market potential of solar systems results not only from environmental aspects, but also from the fact that the prices of solar modules have been dropping over the past few years [1]. Therefore, it is not surprising that PV panels are now commonly used in telecommunications systems as well. Their use in heterogeneous wireless systems, such as mobile networks, turns out to be particularly beneficial.

Wind-generated energy has also been gaining momentum. The amount of energy generated from wind depends mainly on the location, the prevailing weather conditions, and the altitude above sea level at which the installation is operating. Generators harvesting energy from the wind are called wind turbines (WT). A wind turbine converts the energy of wind's velocity into mechanical energy, and then into electrical energy. Wind energy may be a good alternative to solar energy and for some locations or seasons, it may turn out to be an even more reliable power supply solution [2], [3].

Current wireless infrastructure is powered mainly from conventional energy sources that continue to be used on a wide scale. Due to the increasing requirements posed by services rendered with the use of information communication technology (ICT) networks, consumption of and demand for energy continue to grow compared to previous years. By equipping wireless network access points with renewable energy sources (RES), we could greatly reduce or even completely eliminate the need for electricity originating from conventional sources. This, in turn, would not only reduce carbon dioxide (CO_2) emissions but would also slow down the consumption of non-renewable resources. However, despite the many benefits of RES, the big disadvantage is that even and continuous supply of power from such energy resources is not guaranteed due to the changing weather conditions. Therefore, it may be necessary to rely, simultaneously, on more than one type of renewable source or to optimize the use of available energy [2]–[4] by deploying purpose-designed software.

In addition, one of the paradigms applicable to present and future telecommunication systems requires that services need to be available in hard-to-reach and non-populated areas that fail to offer favorable conditions for the development of telecommunication infrastructures, for instance due to terrain configuration or lack of ability to connect to existing telecommunication systems or power sources. Whereas the former problem could be solved by using mobile access nodes (e.g. drones) and relying on wireless connectivity for backhaul communication, the lack of access to a power grid is extremely difficult to overcome [5]. However, an off-grid approach could be adopted to solve this problem, with individual system components powered by RES generators (e.g. solar panels, wind turbines) combined with a battery. Such a configuration could meet the energy demands of a Radio Access Network (RAN) [6]. However, this requires appropriate modeling of the system's energy cycle, i.e. predicting availability of power and the utilization of specific energy resources over time, in such a way as to ensure their adequacy for all types of loads that specific network components are subjected to [7].

In the context of increasing the efficiency of wireless systems, intelligent reflective surfaces (IRSs) are considered to be a highly promising concept. An IRS is a flat-surface device containing a significant number of passive RF reflecting components. Each of these components is capable of independently causing a controlled change in the amplitude and/or phase of the incident radio signal. The dense distribution of IRS surfaces in the wireless network and intelligent coordination of their reflections can make the propagation of the radio signal between transmitters and receivers flexibly reconfigurable. This, in turn, can solve the problems of wireless channel dropouts and interference. In addition, thanks to the use of IRS, improvements in wireless communication solutions' throughput and reliability rates may be achieved as well [8].

This paper presents an energy consumption model for wireless access networks, with its nodes having the form of UAVs equipped with IRSs and powered by RES. In the contribution, the characteristics of the aforementioned system's energy balance, depending on the type of equipment and the prevailing weather conditions, have been investigated as well.

The paper has been organized as follows. In Section 2, analytical models related to energy consumption and harvesting have been described. In Section 3, the simulation setup has been presented. In Section 4, results of the simulation runs performed have been analyzed. Finally, Section 5 focuses on the conclusions and summarized the contribution of the paper.

2. Energy Models

To estimate the energy efficiency of the wireless system under consideration, it is important to precisely configure the setup and to develop an energy cycle model for the network's components. The simulation scenario considered in the paper assumes the use of a UAV – equipped with solar panels and wind turbines for energy generation - serving as a base station. In addition, the mobile access node uses one IRS device to extend the range of the transmitted radio signal and to improve the performance of the wireless system.

The UAV base station may be of the multirotor or fixed-wing type to compare energy balance characteristics of both varieties. The UAV node is able to maintain a connection with the host station via a backhaul link implemented with the use of the microwave technology, and via an access link established using the radio frequency band. The UAV base station freely hovers/flies above the ground, over a city. While a multirotor mobile station can maintain a fixed position in the air, a fixed-wing type station needs to follow a specific flight trajectory. The paper investigates a scenario in which UAVs do not change their position (multirotor) or a trajectory-based flight path (fixed-wing) followed to optimize the location of the UAV station. Verification of the impact that the position of the base station exerts on the functioning of the network is the subject of parallel studies. However, the paper takes into account the impact that the elements – such as wind velocity or cloud cover – have on both the consumption of energy and harvesting energy from RES. Power consumption-related characteristics and the use of energy needed to hover/fly the UAV station determine the availability of services in the considered area using the MIMO technique and thanks to IRS device. However, in the context of obtaining energy from RES, generation-related processes were analyzed with different times of day and year, as well as various wind speeds, solar radiation densities, and types of cloud cover (i.e., different cloud thickness values) taken into consideration. We assume the traffic volume in the telecom network is fixed.

2.1. Energy Consumption Estimation

Power consumption of a fixed-wing UAV mobile base station $(P_{\text{UAV,FW}})$ in time step t can be described by [9]:

$$P_{\text{UAV,FW}}(t) = \left| c_1 v_{\text{UAV}}^3(t) + \frac{c_2}{v_{\text{UAV}}(t)} \left(1 + \frac{a_\perp^2(t)}{g^2}\right) + m_{\text{ALL}} a_\parallel(t) v_{\text{UAV}}(t) \right|, \quad (1)$$

where v_{UAV} is the forward flight velocity of the UAV, $a_\perp$ and $a_\parallel$ are the centripetal acceleration when the base station moves along a circular trajectory, and the forward acceleration, respectively. m_{ALL} is the sum of the masses of all the components of a particular UAV, i.e. the weights of the UAV itself (m_{UAV}), its battery system (m_{BATT}), RES generators $(m_{\text{PV}},\ m_{\text{WT}})$, and additional equipment $(m_{\text{RF}},\ m_{\text{IRS}},\ m_{\text{PKG}})$. Next, the g parameter is the gravitational acceleration, while c_1 and c_2 are the parameters described by [9]:

$$c_1 \triangleq \frac{1}{2}\rho C_{\text{D}_0} S\,, \qquad c_2 \triangleq \frac{2W^2}{\pi e_0 A_{\text{R}} \rho S}\,, \quad (2)$$

where ρ is the air density (calculated according to the formula from [10]), C_{D_0} is the zero-lift drag coefficient and S is the reference area. The $W = m_{\text{ALL}} \cdot g$ parameter stands for the UAV weight force, whereas e_0 and A_{R} are wingspan efficiency (Oswald efficiency) and UAV wing aspect ratio, respectively.

Similarly to the power consumption of multirotor base stations $(P_{\text{UAV,MR}})$ in time step t, its mathematical model is described in the following manner [11]:

$$P_{\text{UAV,MR}}(t) = \frac{d_0}{2}\rho n s A_{\text{UAV}} v_{\text{UAV}}^3(t) + P_0(t)\left(1 + \frac{3v_{\text{UAV}}^2(t)}{\Omega^2(t)R^2}\right) + P_{\text{i}}\tilde{\kappa}(t)\left(\sqrt{\tilde{\kappa}(t) + \frac{v_{\text{UAV}}^4(t)}{4v_0^4}} - \frac{v_{\text{UAV}}^2(t)}{2v_0^2}\right)^{\frac{1}{2}}, \quad (3)$$

where Ω, R, v_0 are the angular velocity, radius and mean induced velocity in the hover mode of a single rotor UAV, respectively. The latter can be expressed as $v_0 = \sqrt{\frac{W}{2\rho A_{\text{UAV}}}}$, where A_{UAV} is the area of the UAV's rotor. The parameters of n and s are the number of UAV rotors and the solidity of a single rotor. $\tilde{\kappa}$ and d_0, in turn, are the UAV's thrust-to-weight ratio and the fuselage drag ratio, respectively. The values of P_0 (in time step t) and P_{i} are described by [11]:

$$P_0(t) = \frac{\delta}{8}\rho n s A_{\text{UAV}} \Omega^3(t) R^3\,,$$
$$P_i = (1+k)\left(\frac{W^3}{2\rho n A_{\text{UAV}}}\right)\,, \quad (4)$$

where δ is the profile drag coefficient and k is the incremental induced power correction factor.

The power used by the IRS device connected to the UAV P_{IRS} and RF transceiver P_{MIMO} has been evaluated in accordance with the mathematical models from [12] and [13], respectively. Those models are described by:

$$P_{\text{IRS}}(t,b) = N(t) \cdot P_{\text{n}}(b)\,, \quad (5)$$

$$P_{\text{MIMO}}(t) = P_{\text{FIX}} + P_{\text{TC}}\big(M(t)\big) + P_{\text{CE}}\big(M(t),K(t)\big) + P_{\text{C/D}}\big(\text{TR}_{\text{UL}}(t),\text{TR}_{\text{DL}}(t)\big) + P_{\text{BH}}\big(\text{TR}_{\text{UL}}(t),\text{TR}_{\text{DL}}(t)\big) + P_{\text{SP}}\big(M(t),K(t)\big) + \frac{P_{\text{TX}}(t)}{\mu_{\text{PA}}}, \quad (6)$$

where P_{FIX} is the fixed power demand of a particular mobile base station, P_{TC} is the consumption of transceiver chains, and P_{CE}, $P_{\mathrm{C/D}}$, and P_{SP} are the power components utilized for operations performed within the base station, such as channel estimation, data coding/decoding, and signal processing.

Next, P_{BH} and P_{TX} are the powers related to mobile data flow, i.e. load-dependent microwave (MW) backhaul and radio frequency (RF) fronthaul, respectively. The parameters of $M(t)$ and $K(t)$ are the numbers of active antenna elements and served users in the current time step t. Next, μ_{PA} is the efficiency of the power amplifier. Finally, the $\mathrm{TR_{UL}}$ and $\mathrm{TR_{DL}}$ components are uplink (UL) and downlink (DL) total data throughputs, which may change over time. In addition, application of the minimum mean-squared error (MMSE) scheme has been assumed for channel estimation and signal processing purposes.

Equation (5) consists of two parameters only, namely N and P_{n}, which are the number of identical reflecting elements responsible for phase shifting on the impinging signal, and the power consumption of each phase shifter, respectively. The value of the latter one depends on the bit resolution b of the used phase shifter type.

2.2. Energy Generation

Energy harvesting models related to the RES generators are presented below. The power generated by the photovoltaic panel of the UAV base station (P_{PV}) can be described by [14]:

$$P_{\mathrm{PV}}(t) = P_{\mathrm{r,PV}} f_{\mathrm{PV}} \frac{\overline{G}_{\mathrm{T}}(t)}{\overline{G}_{\mathrm{T,STC}}} \left[1+\alpha_{\mathrm{P}}\left(T_{\mathrm{c}}(t)-T_{\mathrm{c,STC}}\right)\right], \quad (7)$$

where $P_{\mathrm{r,PV}}$ is the rated capacity of the PV array (its output power under standard test conditions – STC), f_{PV} is the PV derating factor, and α_{P} is the temperature coefficient of power, which indicates how strongly the PV array power output depends on the cell temperature. $\overline{G}_{\mathrm{T}}$ and $\overline{G}_{\mathrm{T,\,STC}}$, in turn, are the solar incident radiation on the PV array in the current time step t and under STC, respectively. T_{c} and $T_{\mathrm{c,STC}}$ are the PV cell's temperature in the current time step t and under STC, respectively. The PV cell temperature can be calculated with the equation contained in [14].

The power generated by the wind turbine P_{WT} can be described as [15]:

$$P_{\mathrm{WT}}(t) = \begin{cases} 0, & \text{if } v_{\mathrm{w}}(t) < v_{\mathrm{in}} \\ F\left(v_{\mathrm{w}}(t)\right), & \text{if } v_{\mathrm{in}} \leqslant v_{\mathrm{w}}(t) < v_{\mathrm{r}} \\ P_{\mathrm{r,WT}}, & \text{if } v_{\mathrm{r}} \leqslant v_{\mathrm{w}}(t) \leqslant v_{\mathrm{out}} \end{cases}, \quad (8)$$

where v_{in}, v_{out}, v_{w} are the cut-in and cut-out speeds of the wind turbine, defining the range of wind velocity values for which the wind turbine is able to generate energy, and the instantaneous wind speed, respectively. Next, F is the power curve function of the WT, which determines its energy harvesting properties. Finally, $P_{\mathrm{r,WT}}$ and v_{r} denote the rated output power of the wind turbine used and the minimum wind speed $v_{\mathrm{in}} < v_{\mathrm{r}} < v_{\mathrm{out}}$ at which this power can be generated, respectively. The power curve function normalized in the relation to the maximum value of the WT's output power has been presented in Fig. 1. The corrections of wind speed (to get its correct value at the altitude of the generator) and the WT power (which depends on the current air density) were realized in accordance with [14].

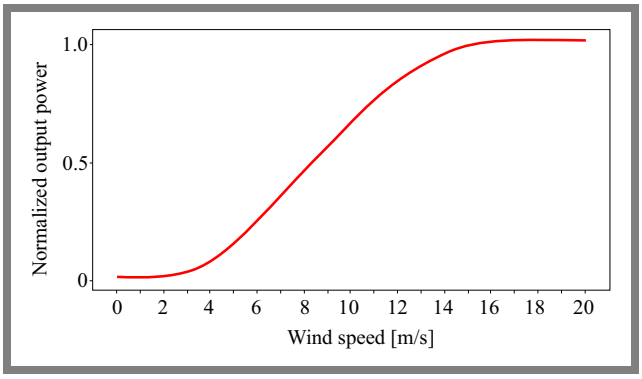

Fig. 1. Power curve function of wind turbine based on [16].

3. Simulation Setup

The researched base stations had the form of multirotor and fixed-wing type UAVs. Furthermore, each UAV BS was also equipped with a single RF transceiver and an IRS device. The impact of RES generators on the overall power consumption (PC) of the mobile base station has been taken into consideration as well. Thus, four different scenarios have been simulated. The first case investigates PC in different seasons of the year, i.e. power used by the UAV and its additional equipment – IRS device and the RF transceiver – with no RES generators on board. The second, third, and fourth cases take into account as well the power consumed by the mobile BS with a PV, a WT, and both devices, respectively. Amounts of energy generated by RES have been obtained based on values describing actual products, with their specifications found in [16] and [17].

The simulations have been conducted using the Python programming language. Energy consumption characteristics of the mobile base stations, as well as the amounts of energy harvested from RES generators have been evaluated. The results have been prepared for four different dates marking the beginning of different seasons of the year – vernal equinox (20th March 2022), summer solstice (21st June 2022), autumn equinox (23rd September 2022), and winter solstice (21st December 2022). All the weather-related values used in the simulations are actual historic data obtained from [18] for the city of Poznań (Poland). Global solar radiation density is the only exception, as it was estimated using the MAC model from [19].

All the energy characteristics charts compiled have been normalized in relation to the maximum values obtained. Furthermore, in Tab. 1, the values of parameters used in the mathematical energy models discussed in Section 2 have been highlighted. The values of parameters related to the RF transmission power consumption model, not shown in Tab. 1, were taken from Tab. 5.3 in [13].

Tab. 1. Simulation parameters retrieved from [7], [9], [11], [12], [16], [17], [20]–[23].

Symbol	Description	Value	Unit
m_{UAV}	Mass of a UAV	5.0	kg
m_{BATT}	Mass of a battery	0.94	kg
m_{RF}	Mass of a RF transceiver	2.0	kg
m_{IRS}	Mass of an IRS device	1.0	kg
m_{PV}	Mass of a PV panel	2.78	kg
m_{WT}	Mass of a WT	6.0	kg
m_{PKG}	Mass of an additional package	0.0	kg
Ω	Rotor angular velocity	300.0^{*}	rad/s
v_{UAV}	Velocity of a UAV	0.0^{*}, 10.0^{**}	m/s
v_{in}	Cut-in speed of a WT	2.0	m/s
v_{out}	Cut-out speed of a WT	20.0	m/s
v_{r}	Rated speed of a WT	16.0	m/s
$a_{\parallel}$	UAV's forward acceleration	0.0^{**}	$\mathrm{m/s^2}$
$a_{\perp}$	UAV's centripetal acceleration	0.0^{**}	$\mathrm{m/s^2}$
g	Gravitational acceleration	9.81	$\mathrm{m/s^2}$
δ	Profile drag coefficient	0.012^{*}	
k	Increment correction factor	0.1^{*}	
$\tilde{\kappa}$	Thrust-to-weight ratio	1^{*}	
d_0	Fuselage drag ratio	14.52^{*}	
$C_{\mathrm{D_0}}$	Zero-lift drag coefficient	0.01^{**}	
e_0	Oswald efficiency	0.85^{**}	
A_{R}	UAV's wing aspect ratio	118.81^{**}	
S	UAV's ref. (wing) area	1.0^{**}	$\mathrm{m^2}$
A_{UAV}	UAV's rotor area	0.071^{*}	$\mathrm{m^2}$
R	UAV's rotor radius	0.15^{*}	m
s	UAV's rotor solidity	0.067^{*}	
n	Number of rotors	8^{*}	
M	Number of antenna elements	16	
K	Number of users	10	
N	Number of reflecting elements	16	
b	Phase shifter resolution	6	bit
$\mathrm{TR_{UL}}$	UL data throughput	50.0	Mbps
$\mathrm{TR_{DL}}$	DL data throughput	100.0	Mbps
f_{PV}	PV's derating factor	0.72	
α_{P}	Temperature coefficient of power	-0.5	%/°C
$T_{\mathrm{c,STC}}$	STC solar cell temperature	25	°C
$G_{\mathrm{T,STC}}$	STC solar incident radiation	1000	W
$P_{\mathrm{r,PV}}$	PV panel's rated power	20.0	W
$P_{\mathrm{r,WT}}$	Rated power of a WT	30.0	W
P_{n}	Power of a phase shifter	7.8	W
P_{TX}	UAV transmit power	15.0	W
μ_{PA}	Power amplifier efficiency	0.35	

* for the multirotor type only, ** for fixed-wing type only

4. Results

Here, charts presenting energy consumption characteristics of mobile base stations, as well as amounts of energy generated by their RES are shown. Specific colors used in the plots are strictly associated with a specific season of the year: blue – vernal equinox, yellow – summer solstice, green – autumn equinox, and red – winter solstice.

In Fig. 2, the normalized energy utilization process for the different UAV types is presented. The chart at the top shows the characteristics of a multirotor UAV, while the one visible below identifies the amount of energy consumed by the fixed-wing type UAV. The values presented in the figure were not normalized in the relation to the same value, but each one was scaled according to the maximum value obtained for a particular scenario. Thus, lower consumption values observed for the multirotor type do not mean this type of UAV uses less energy than the fixed-wing variety.

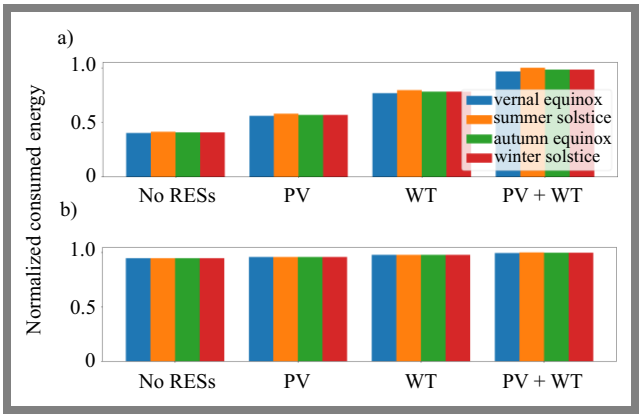

Fig. 2. Energy consumption characteristics for: a) multirotor and b) fixed-wing UAVs.

The main goal of the investigation was to highlight the impact that adding extra equipment to the UAV's weight has on the amount of energy it uses in different seasons of the year. In the case of a hovering multirotor UAV, its total weight has a crucial influence on its energy demand. With a PV panel and a wind turbine (approx. 9 kg) added to the BS, its energy consumption increases almost by a factor of two. Some variations in the amounts of energy used by the multirotor UAV may be observed during different seasons of the year as well. This is caused by the fact that air density fluctuates during the year. For the fixed-wing type UAV, the aforementioned weight- and weather-related dependencies may be noticed as well, but their impact on PC is not as significant as in the case of the multirotor BS. On the other hand, only one case has been considered in this paper, in which the fixed-wing UAV was flying with a constant velocity of 10 m/s. The real impact might be assessed by studying changes in the amount of energy used by the UAV lifting various loads from the ground, or by studying changes in its aerodynamic characteristics. Both cases will be considered in future work.

Figure 3 presents the energy generation processes of PV panels and wind turbines used to augment the power supply of UAV BSs. The characteristics have been derived from real world equipment specifications from [16] and [17]. Figure 3 highlights energy gains that may be achieved during different seasons of the year. Based on that data, one may assess when equipping a mobile base station with a specific RES generator is beneficial. For instance, in the summer, a PV panel is the

most effective and a WT is the least efficient solution. In winter, however, the opposite is true.

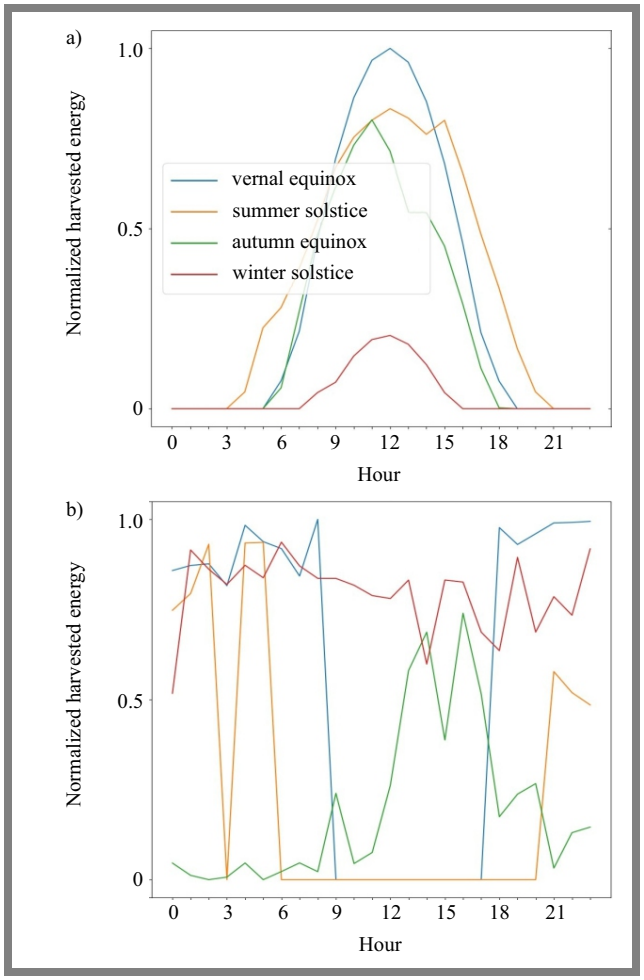

Fig. 3. Energy generation characteristics for PV panels and wind turbines.

Interestingly, the amount of energy produced by both generators is at its peak close to the vernal equinox, although this particular time of year is not the most effective season for producing power with the use of PV panels or wind turbines. This stems from the limitations of RES generators, i.e. each type has optimal temperature or/and wind speed ranges in which it is capable of producing the largest amount of renewable energy. The output power of PV panels is greatly influenced by the current temperature of solar cells – a value that depends on current ambient temperature and cloud opacity. Thus, an increase in air temperature and cloud coverage may cause a decrease in the efficiency of the energy generation process.

5. Conclusions

In this paper, energy use and generation characteristics of two types of UAV mobile base stations equipped with RF transceivers, IRS devices, and RES generators (PV panels and wind turbines) have been investigated. The results obtained highlight the impact that the UAV's equipment has on the energy balance in different seasons of the year. The findings identified in this paper seem to be valuable for the process of planning networks used in future wireless systems relying on UAVs, IRSs, and RES.

Acknowledgments

The work has been performed within the framework of research project no. 2021/43/B/ST7/01365 funded by that National Science Center in Poland.

References

[1] V. Kozlov and W. Salabun, "Challenges in reliable solar panel selection using MCDA methods", *Procedia Computer Science*, vol. 192, pp. 4913–23, 2021 (https://doi.org/10.1016/j.procs.2021.09.269).

[2] A. Jahid, M.K.H. Monju, M.E. Hossain, and M.F. Hossain, "Renewable energy assisted cost aware sustainable off-grid base stations with energy cooperation", *IEEE Access*, vol. 6, pp. 60900–60920, 2018 (https://doi.org/10.1109/ACCESS.2018.2874131).

[3] M. Deruyck *et al*., "Designing a hybrid renewable energy source system to feed the wireless access network", *Sustainable Energy, Grids and Networks*, vol. 31, 2022 (https://doi.org/10.1016/j.segan.2022.100722).

[4] A. Samorzewski and A. Kliks, "User allocation in heterogeneous network supplied by renewable energy sources", 2021 *17th International Conference on Wireless and Mobile Computing, Networking and Communications* (*WiMob*), Bologna, Italy, pp. 419–422, 2021 (https://doi.org/10.1109/WiMob52687.2021.9606428).

[5] A. Chaoub *et al*., "6G for bridging the digital divide: Wireless connectivity to remote areas", *IEEE Wireless Communications*, vol. 29, no. 1, pp. 160–168, 2022 (https://doi.org/10.1109/MWC.001.2100137).

[6] M.S. Hossain *et al*., "Towards energy efficient load balancing for sustainable green wireless networks under optimal power supply", *IEEE Access*, vol. 8, pp. 200635–200654, 2020 (https://doi.org/10.1109/ACCESS.2020.3035447).

[7] O. Arnold, F. Richter, G.P. Fettweis, and O. Blume, "Power consumption modeling of different base station types in heterogeneous cellular networks", in *2010 Future Network & Mobile Summit*, Florence, Italy, 2010

[8] Q. Wu, S. Zhang, B. Zheng, C. You, and R. Zhang, "Intelligent reflecting surface-aided wireless communications: A tutorial", *IEEE Transactions on Communications*, vol. 69, no. 5, pp. 3313–3351, 2021 (https://doi.org/10.1109/TCOMM.2021.3051897).

[9] Y. Zeng and R. Zhang, "Energy-efficient UAV communication with trajectory optimization", *IEEE Transactions on Wireless Communications*, vol. 16, no. 6, pp. 3747–3760, 2017 (https://doi.org/10.1109/TWC.2017.2688328).

[10] D. Czernia and B. Szyk, "Air density calculator" [Online]. Available: (https://www.omnicalculator.com/physics/air-density (accessed: 21 March 2023).

[11] Y. Zeng, J. Xu, and R. Zhang, "Energy minimization for wireless communication with rotary-wing UAV", *IEEE Transactions on Wireless Communications*, vol. 18, no. 4, pp. 2329–2345, 2019 (https://doi.org/10.1109/TWC.2019.2902559).

[12] C. Huang, A. Zappone, G.C. Alexandropoulos, M. Debbah, and C. Yuen, "Reconfigurable Intelligent Surfaces for Energy Efficiency in Wireless Communication", IEEE Transactions on Wireless Communications, vol. 18, no. 8, pp. 4157–4170, 2019 (https://doi.org/10.1109/TWC.2019.2922609).

[13] E. Björnson, J. Hoydis, and L. Sanguinetti, "Massive MIMO networks: Spectral, energy, and hardware efficiency", *Foundations and Trends in Signal Processing*, vol. 11, no. 3–4, pp. 154–655, 2017 (http://dx.doi.org/10.1561/2000000093).

[14] HOMER Pro v3.15, "Documentation – HOMER's Calculations" [Online]. Available: https://www.homerenergy.com/products/pro/docs/3.15/homers_calculations.html (accessed: 21 March 2023).

[15] C. Carrillo, A.F. Obando Montaìo, J. Cidrçs, and E. Díaz-Dorado, "Review of power curve modelling for wind turbines", *Renewable and Sustainable Energy Reviews*, vol. 21, pp. 572–581, 2013 (https://doi.org/10.1016/j.rser.2013.01.012).

[16] "Saiam VAWT SAV-30W Specifications" [Online]. Available: http://www.yashikaenergy.com/pdf/sai3.pdf (accessed: 21 March 2023).

[17] "Solarland SLP020-12U Specifications & Warranty" [Online]. Available: https://www.solar-electric.com/lib/wind-sun/SLP020-12U.pdf (accessed: 21 March 2023).

[18] Visual Crossing, "Historical Weather Data & Weather Forecast Data" [Online]. Available: https://www.visualcrossing.com/weather-data (accessed: 21 March 2023).

[19] J.A. Davies and D.C. McKay, "Estimating solar irradiance and components", *Solar Energy*, vol. 29, no. 1, pp. 55–64, 1982 (https://doi.org/10.1016/0038-092X(82)90280-8).

[20] E.A. Franklin, "Calculations for a Grid-Connected Solar Energy System" [Online]. Available: https://extension.arizona.edu/sites/extension.arizona.edu/files/pubs/az1782-2019.pdf (accessed: 21 March 2023).

[21] Green Cell, "Green Cell Accumulator LiFePO4 12V 12.8V 7Ah – Product card CAV09" [Online]. Available: https://greencell.global/en/index.php?controller=attachment&id_attachment=316 (accessed: 21 March 2023).

[22] "HOMER Pro v3.15, Documentation – Glossary" [Online]. Available: https://www.homerenergy.com/products/pro/docs/3.15/glossary.html (accessed: 21 March 2023).

[23] F. Götten, D.F. Finger, M. Havermann, and C. Braun, "Full configuration drag estimation of short-to-medium range fixed-wing UAVs and its impact on initial sizing optimization", *CEAS Aeronautical Journa*l, vol. 12, no. 6, pp. 589–603, 2021 (https://doi.org/10.1007/s13272-021-00522-w).

Adam Samorzewski, M.Sc.
https://orcid.org/0000-0003-4138-5544
E-mail: adam.samorzewski@doctorate.put.poznan.pl
Institute of Radiocommunications, Poznań University of Technology, Poznań, Poland